Analytical Chemistry

Preparation and Performance Study of Antibacterial Materials Based on GO–TiO_2

Hongxia Li,[a] Jie Wu,[a] Xiang Gao,[a] Tiantian Li,[a] Mengmeng Zhang,[a] Xiaohui Niu,[a] Deyi Zhang,[a] Yi Wang,[a] Haiyan Fan,[b] and Kunjie Wang*[a]

A composite of graphene oxide (GO) and titanium (IV) oxide was prepared through a hydrothermal treatment by mixing TiO_2 with GO. The GO was obtained by using an improved Hummers' method. The composite (TiO_2-GO) only indicated a weak antibacterial effect against Escherichia coli under dark conditions. Upon introduction of silver-based nanomaterials, two new composites viz. GO–TiO_2–Ag and GO–TiO_2–Ag_2S were prepared also through hydrothermal reaction. While both composites exhibit stronger antibacterial activities against *E. coli* than TiO_2-GO in dark, GO–TiO_2–Ag composite exhibited higher bactericidal rate (92%) than GO–TiO_2–Ag_2S (40%).

1. Introduction

The high mortality rate caused by bacterial infections has become a serious health problem.[1] Antibiotics have become most popular antibacterial agents to fight against various bacterial infections. However, substantial class of antibiotics target DNA or RNA those are play important roles in bacterial cell wall and /or cell membrane growth, thus causing inevitable drug resistance.[2,3] Nanostructured oxides, such as TiO_2, CuO, ZnO and Al_2O_3, have been reported and had an important influence on the cell structure of bacteria, fungi, viruses and other biological microorganisms due to their high specific surface area.[4–6] Among these metal oxides, TiO_2 nanoparticles (NPs) has been widely studied due to its high stability and broad-spectrum antibacterial properties.[7] So far, antibacterial properties of TiO_2 can be attributed to its excellent photo-activation properties. Photo-generated electrons and holes that can potentially help to produce active oxygen and kill bacteria.[8–10] In the absence of light, it was found that TiO_2 can alter the bacterial cell wall morphology and permeability, thereby regulate the osmotic balance of bacteria.[6,11–13]

Among the carbon-based nanomaterial with antimicrobial properties, graphene oxide (GO) has received extensive attention due to its unique physical and chemical properties. The mechanisms of its antibacterial activity include physical/mechanical damage and oxidative stress.[14] With its blade/knife-like morphology, GO can destroy bacterial cell wall/membrane via its strong mechanical stress. Such mechanism was confirmed in the measurement of the released bacterial cell components (such as RNA) in phosphate buffer.[15] On the other hand, through a surface modification, graphene derivatives show antibacterial effects by generating Reactive Oxygen Species (ROS). Antimicrobial effects of GO and RGO based on ROS-associated oxidative stress have been observed on the model bacteria such as *Xanthomonas oryzae* pv. *oryzae* and *Pseudomonas* aeruginosa.[16,17]

The composite of TiO_2 and GO possess morphology of a planar monolayer of carbon atoms densely packed in a two-dimensional (2D) honeycomb lattice, and the nanoparticles of TiO_2 were evenly dispersed. The composite materials of GO and TiO_2 have indicated unique physical, chemical and mechanical properties,[18] and visible light-induced antibacterial effects.[19] However, little attention has been paid on the antibacterial properties of GO and TiO_2 composite materials in the dark.

Antibacterial effect of silver[20] has been identified since ancient time.[21,22] In current time, silver has been used as antibacterial agents in various areas, including dental work, catheters, and burn wounds.[23,24] As the matter of fact, up to 12 kinds of E. coliinorganic antibacterial agents rely on the cytotoxicity of silver ions and silver-based compounds are very toxic toward microorganisms.[25,26] In this work, we attempted to synthesize GO–TiO_2–Ag and GO–TiO_2–Ag_2S composites through an in-situ growth method by taking advantage of strong antimicrobial effecting of silver-based nanomaterials and the large surface area of GO, which was helpful to dope TiO_2. We synthesized GO–TiO_2–Ag and GO–TiO_2–Ag_2S composite materials to achieve stronger antibacterial effects and avoid potential drug resistance.

Experimental

Materials

The experimental reagent used in this article are as follows: butyl titanate (Tianjin Damao Chemical Reagent Factory), silver nitrate (Tianjin Damao Chemical Reagent Factory), sodium sulfide (Yantai Shuangshuang Chemical Reagent Company), graphite powder (Aladdin Industrial Company), Peptone (Shanghai Zhongqin Chem-

[a] Dr. H. Li, J. Wu, X. Gao, T. Li, M. Zhang, X. Niu, D. Zhang, Y. Wang, K. Wang
School of Petrochemical Engineering,
Lanzhou University of Technology,
Lanzhou 730050, China
E-mail: wangkj80@163.com
[b] H. Fan
Chemistry Department,
Nazarbayev University,
Astana 010000, Kazakhstan

ical Reagent Co., Ltd.), sodium hydroxide (Sinopharm Group Chemical Reagent Co., Ltd.), agar powder (Beijing Aoboxing Biotechnology Co., Ltd.), beef extract (Beijing Shuangxuan Microbiological Culture Medium Products Factory), potassium permanganate (Tianjin BASF Chemical Co., Ltd.), dichloromethane (Tianjin Kaixin Chemical Co., Ltd.) carbon tetrachloride (Sino Pharmaceutical Holdings Chemical Reagent Co., Ltd.). The water used in all experiments was ultrapure water, and all the chemical reagents used are analytically pure.

Preparation of GO–TiO_2–Ag

1 g of the prepared GO was added to 200 mL of distilled water and sonicate for 30 minutes to obtain a uniform suspension. After adding appropriate amount ethanol solution of butyl titanate dropwise to the suspension, the mixture was transferred to a 100 mL reactor and reacted at 150 °C for 10 h. Upon cooling, the precipitate was dissolved again in 30 mL of distilled water under constant stirring. 0.17 g $AgNO_3$ was added and let reacted at 40 °C for 12 h. Upon completion of the reaction, the product was filtered, washed several times and dried in a vacuum oven at 60 °C to obtain GO–TiO_2–Ag powder.

(a) Strain activation and preparation of suspension

Bacterial species activation: In an ultra-clean operating station, select colonies from two inclined plane cultures with the inoculation ring to inoculate into their respective suitable liquid culture medium, and the bacteria were cultivated in a constant temperature incubator at 37 °C for 24 h.

Preparation of bacterial suspension: place activated bacterial species in a vial of sterile water and shake well to prepare a suspension of the bacterial species. Place incubator in a water bath thermostat. Draw 0.1 mL of the prepared bacterial suspension and add to a small centrifuge tube, then diluted to 1 mL; repeat this process for 10 times. After culturing in the respective solid medium, count the bacteria and determine the optimal gradient.

(b) Antibacterial performance test

1 mg/mL GO–TiO_2, GO–TiO_2–Ag and GO–TiO_2–Ag_2S suspensions was added to the test tube and mix with 10^5-10^6 CFU/mL *E. coli* 0.9% saline. Gram-negative *E. coli* containing only 0.9% saline was used as a control. All samples were shacked in a constant temperature at 37 °C, spreading them evenly on LB solid medium. Then they were incubated in a constant temperature incubator at 37 °C for 24 h. The number of colonies forming units (CFU) was calculated. The antibacterial activity is expressed as the percentage of microorganism reduction (R%), according to the following formula:

$$R\% = (A-B)/A \times 100\%$$

Where A and B represent the concentration (CFU/mL) of untreated and treated samples measured at the specified contact time, respectively.

2. Results and discussion

2.1. Structure and Chemical Composition

XRD pattern of GO (figure 1a) shows a sharp diffraction peak at $2\theta = 10.6°$ with strong intensity, indicating that the graphite has been oxidized to graphene oxide. In XRD pattern of GO–TiO_2 (Figure 1b), characteristic peaks was centered at $2\theta =$

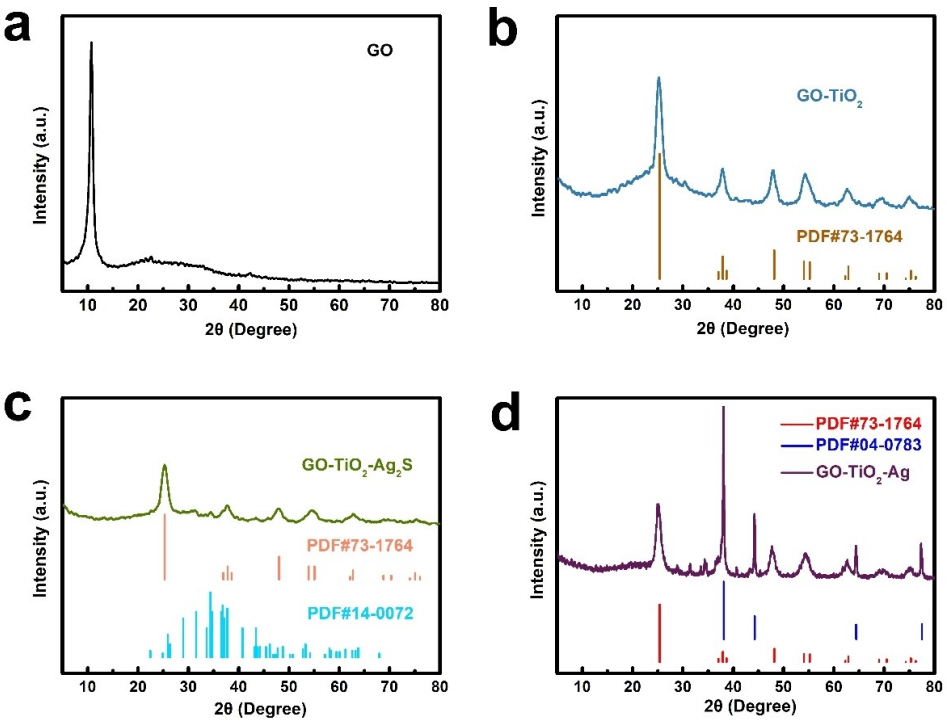

Figure 1. XRD spectrum of (a) GO (b) GO–TiO_2 (c) GO–TiO_2–Ag_2S (d) GO–TiO_2–Ag

25.3°, 37.7°, 48.1°, 54.5° and 62.8°, which are identified as TiO_2 (PDF#73-1764), but the characteristic peak on GO was disappeared. In the XRD pattern of GO–TiO_2–Ag_2S composite (Figure 1c), all the characteristic peaks for TiO_2 remain but with much weaker intensities, the peak for GO disappears, and a peak at $2\theta = 37.9°$ appears representing Ag_2S. The fact that the characteristic diffraction peaks of TiO_2 exhibit low intensity and no diffraction peak for GO is shown for GO–TiO_2–Ag_2S composite is likely due to some intrinsic interaction among GO, TiO_2 and Ag_2S wherein each compound coordinates with one another. Figure 1d displayed the same diffraction pattern for the (101), (004), and (200) crystal planes of anatase TiO_2 (PDF#73-1764). In addition, a diffraction peak at $2\theta = 38.29°$ is identified as (111) crystal plane of Ag element (PDF#04-0783).

The SEM image of GO (Figure 2a) indicates some thin sheet like morphology with smooth surface and folds. Some wrinkles can be observed on the edge of the thin sheet representing a small amount of graphene oxide layer. The SEM image of GO–TiO_2 (Figure 2b) exhibits small particles of TiO_2 that are dispersed on the surface of GO sheet. The SEM images of GO–TiO_2–Ag_2S and GO–TiO_2–Ag depicted in Figure 2c and Figure 2d respectively, demonstrating a similar morphology to that of GO–TiO_2 except the particles distributed on the GO sheet are generally grow a little bit in size due to the addition of Ag_2S or Ag.

HRTEM images of GO–TiO_2–Ag in Figure 3a exhibit an obvious crystal plane stripes, indicating a good crystallinity. The spacing of lattice fringes ($d = 0.355$) is coincident with the (220) crystal plane spacing of anatase TiO_2, which was identified in the XRD spectra. Figure 3b shows that the TiO_2 nanoparticles are distributed on the GO, and the darker colored Ag NPs are also dispersed on the flakes of GO and mostly in the area which are TiO_2 nanoparticles. In Figure, the folds on GO are visible, just like what observed in SEM. The electron diffraction pattern (SAED) of the composite GO–TiO_2–Ag in the selected area is displayed in Figure 3d, the diffraction ring is identified illustrating the polymorphism of the sample. Such is an indication that the composite GO–TiO_2–Ag were successfully prepared.

The XPS survey spectrum of GO–TiO_2–Ag_2S indicates the elements (O, Ti, Ag, C, S) in this sample are in the ratio of O:Ti:Ag:C:S = 28.02:6.65:3.23:60.31:1.79 (Figure 4a). Two character peaks at 464.63 eV and 458.78 eV in the high resolution XPS spectrum are corresponding to Ti 2p, which are assigned as Ti $2p_{1/2}$ and Ti $2p_{3/2}$ in the form of Ti^{4+}.[27] The deconvolved Ag 3d peaks in Figure 4c at 367.3 eV and 373.4 eV are identified as the energy values of Ag $3d_{5/2}$ and Ag $3d_{3/2}$.[28,29]

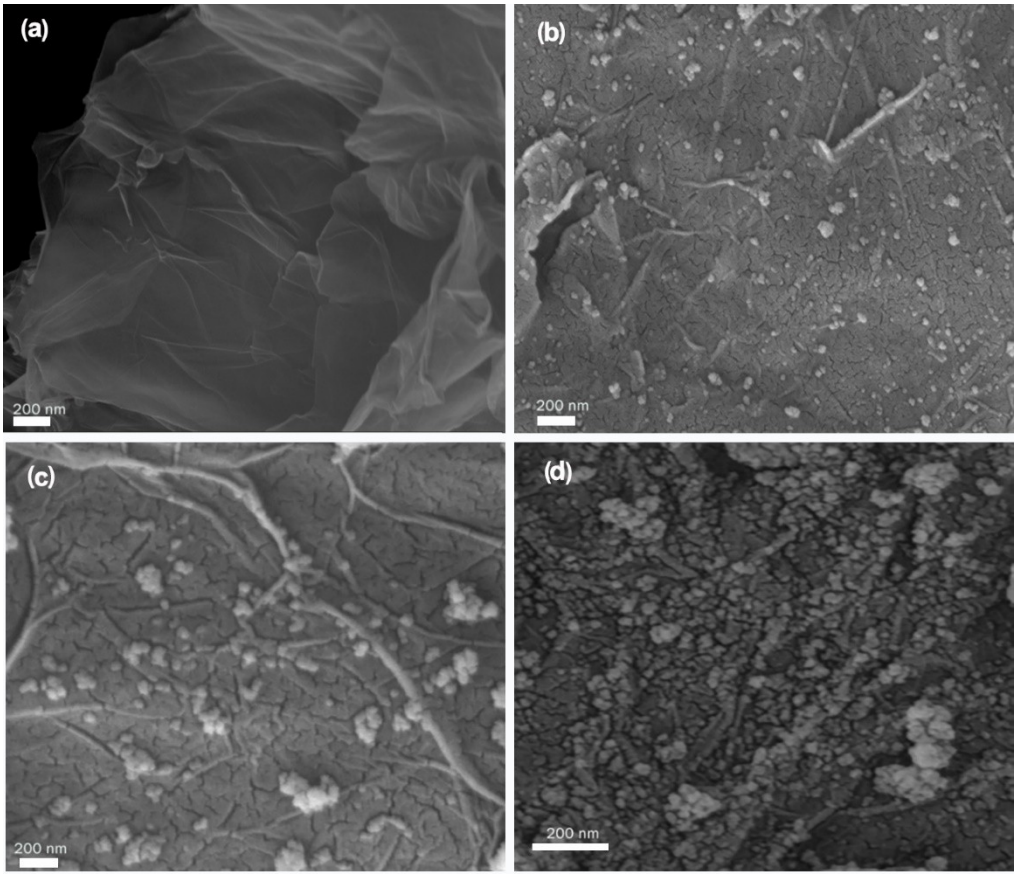

Figure 2. SEM spectrum of (a) GO (b) GO–TiO_2 (c) GO–TiO_2–Ag_2S (d) GO–TiO_2–Ag

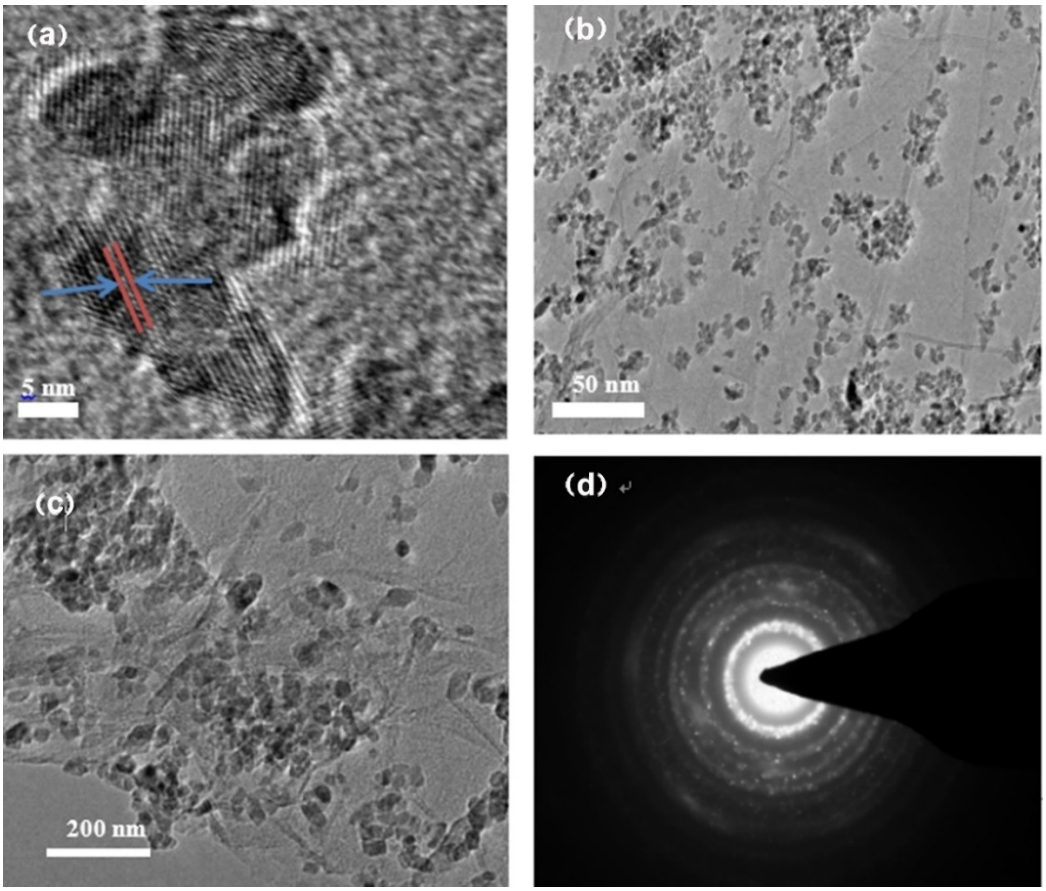

Figure 3. (a) ~ (c) are the TEM spectra of GO–TiO_2–Ag (d) SAED diagram

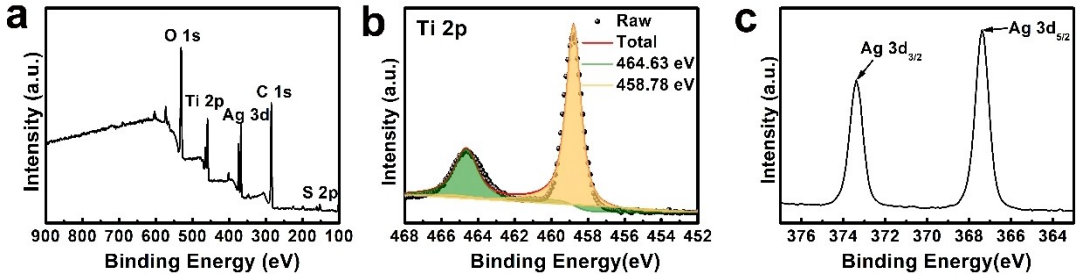

Figure 4. (a) Total spectrum of GO–TiO_2–Ag_2S (b) Fitting diagram of Ti 2p in GO–TiO_2–Ag_2S (c) Magnified XPS spectrum of Ag 3d

2.2. Antimicrobial activity

The antibacterial performance of GO–TiO_2 showed in Figure 5(b) is poor in dark, mainly because the antibacterial effect of TiO_2 is based on its photosensitivity. On the other hand, the sheets of GO with relatively large area, which can cover the bacteria and prevent them from ingesting nutrients, resulting in weak antibacterial performance. Compared to GO–TiO_2, GO–TiO_2–Ag_2S have improved inhibition against *E. coli*, the antibacterial effect observed for GO–TiO_2–Ag_2S composite remains weak due to the slow release of silver ions from Ag_2S and less damage to bacteria in a shorter period. GO–TiO_2–Ag composite showed the best antibacterial effects mainly initiated by the positive charged Ag nanoparticles distributed on the surface of composite to attach to the bacterial cell membranes. Once silver ions are released, which can facilitate the production of ROS and free radicals that cause dysfunction of key cell components.

Three sets of parallel tests were performed and the antibacterial rate of different composite materials were calculated based on the number of bacterial colonies obtained after 24 hours of incubation at 37 °C. The antibacterial rate for GO–TiO_2, GO–TiO_2–Ag_2S and GO–TiO_2–Ag was found 14%, 40% and 92% respectively (Table 1). And according to the

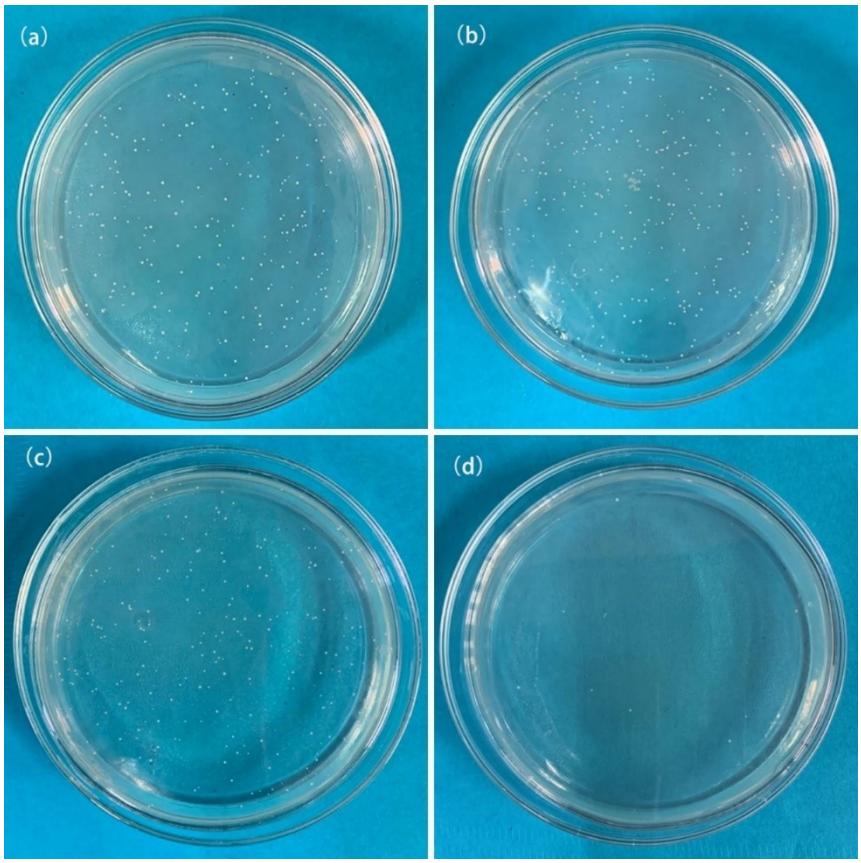

Figure 5. (a)*E. coli* control group (b)GO–TiO_2 bacteriostatic effect diagram (c) GO–TiO_2–Ag_2S bacteriostatic effect diagram (d) GO–TiO_2–Ag bacteriostatic effect diagram

Table 1. Antibacterial rate of different composite materials.

	Compounds	Average number of colonies(a)	Average bacteriostatic rate(%)
E.coli	Control	250	–
	GO–TiO_2	215	14
	GO–TiO_2–Ag_2S	150	40
	GO–TiO_2–Ag	20	92

obtained data, a histogram of the antibacterial rate of different composite materials against *E. coli* was made (Figure 6). The antibacterial rate against *E. coli* indicated by GO–TiO_2–Ag prepared in the present work is 1.7 times larger than that of AgNP-MgO–TiO_2 material.[12]

2.3. Antimicrobial mechanism

The antibacterial results showed that the GO–TiO_2 composite material has weak antibacterial performance in the dark. The particles TiO_2 partially aggregated on the surface of the bacteria to inactivate the bacteria.[11] Meanwhile, the flaky GO can also cause some damage to the bacteria.[15,30] The antibacterial activity of the GO–TiO_2–Ag_2S composite material is improved because of the introduction of Ag_2S. Ag_2S has ability to release Ag^+, and react with the negatively charged bacterial outer membrane as well as the negatively charged phosphate easter on cell wall, consequently destroy the integrity of the bacteria. However, due to the low speed of Ag^+ releasing, antibacterial activity was not obvious till 24 h treatment.[31] The presence of Ag NPs on the surface of GO–TiO_2–Ag composite material greatly enhances the antibacterial activity. Ag NPs can not only destroy the outer membrane of the bacteria, but also generate ROS, thus causing damage to the bacteria.[32] Meanwhile the particles of TiO_2 are able to enter the bacterial cell through the disrupted cell membrane, and destroy the internal organelles of the bacteria. A diagram describing the antibacterial mechanism is shown in Figure 7.

3. Conclusions

In the present work, graphene oxide was prepared by an improved Hummers method, and TiO_2 nanoparticles were successfully loaded on the surface of the GO sheet through a hydrothermal treatment at 50 °C. In order to enhance the antibacterial effect, Ag_2S and Ag NPs were introduced to form complexes GO–TiO_2–Ag_2S and GO–TiO_2–Ag, respectively. The as prepared materials, viz. GO–TiO_2–Ag, GO–TiO_2–Ag_2S and GO–TiO_2 all indicated antibacterial effect against E. coli with the antibacterial rate of 92%, 40% and 14%, respectively. The

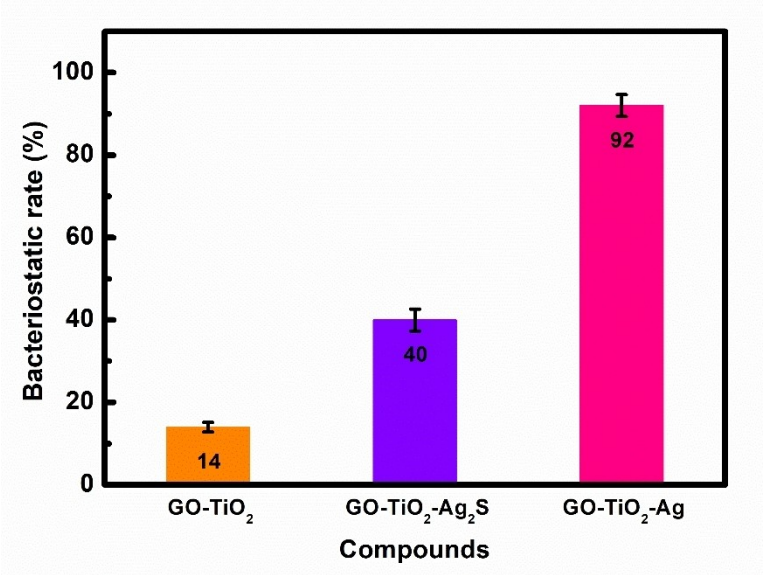

Figure 6. Antibacterial rate of different composite materials, error bars show the standard deviation of the three experimental results.

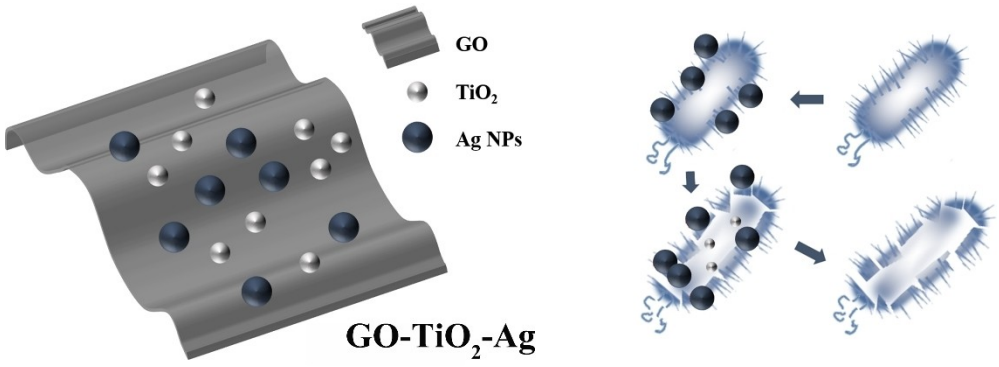

Figure 7. Antibacterial mechanism diagram of GO–TiO2–Ag composite material.

mechanism analysis revealed the composites containing Ag_2S or Ag NPs can potentially destroy the bacterial cell membrane and internal organelles. The present study provides a simple methodology to synthesize Ag containing composites that possess strong antimicrobial effect against Gram-negative bacteria like *E. coli*.

Supporting Information

See the supporting information for the synthesis methods of GO, GO–TiO_2 and GO–TiO_2–Ag_2S.

Acknowledgements

This work was supported by the National Nature Science Foundations of China (Grants No. 21867015, 22065021), the Province Nature Science Foundations of Gansu (Grants No. 20JR5RA453) and Hongliu Outstanding Youth Teacher Cultivate Project of Lanzhou University of Technology.

Conflict of Interest

The authors declare no conflict of interest.

Keywords: Antibacterial · Graphene oxide · Silver-based nanomaterials · Titanium dioxide

[1] R. J. Melander, D. V. Zurawski, C. Melander, *MedChemComm* **2018**, *9*, 12–21.
[2] K. E. Jones, N. G. Patel, M. A. Levy, A. Storeygard, D. Balk, J. L. Gittleman, P. Daszak, *Natur* **2008**, *451*, 990–997.
[3] M. Gheorghiade, G. Filippatos, L. De Luca, J. Burnett, *Am. J. Med.* **2006**, *119*, S3-S10.
[4] K. K. Dey, A. Kumar, R. Shanker, A. Dhawan, M. Wan, R. R. Yadav, A. K. Srivastava, *RSC Adv.* **2012**, *2*, 1387–1403.
[5] L. Yu, J. Li, D. Wang, L. Ouyang, G. Jin, X. Liu, *Mater. Technol.* **2015**, *30*, B109-B114.
[6] R. Verma, V. Chaudhary, L. Nain, A. Srivastava, *Mater. Technol.* **2017**, *32*, 385–390.
[7] S. K. Kassahun, Z. Kiflie, H. Kim, B. T. Gadisa, *J. Environ. Chem. Eng.* **2020**, *8*, 104374.

[8] B. Moongraksathum, Y. W. Chen, *Catal. Today* **2017**, 310, 68–74.
[9] R. Kaushik, P. K. Samal, A. Halder, *ACS App. Nano Mater.* **2019**, *2*, 7898–7909.
[10] I. Milosevic, A. Jayaprakash, B. Greenwood, B. Van Driel, S. Rtimi, P. Bowen, *Nanomater.* **2017**, *7*, 391.
[11] J. Nesic, S. Rtimi, D. Laub, G. M. Roglic, C. Pulgarin, J. Kiwi, *Colloids Surf. B* **2014**, *123*, 593–599.
[12] T. Jaiakumar, M. Umadevi, J. Mayandi, G. Sathe, *Mater. Lett.* **2016**, *184*, 82–87.
[13] I. Fenoglio, G. Greco, S. Livraghi, B. Fubini, *Chem. A Eur. J.* **2009**, *15*, 4614–4621.
[14] Q. Xin, H. Shah, A. Nawaz, W. Xie, M. Z. Akram, A. Batool, L. Tian, S. U. Jan, R. Boddula, B. Guo, *Adv. Mater.* **2019**, *31*, 1804838.
[15] O. Akhavan, E. Ghaderi, *ACS Nano* **2010**, *4*, 5731–5736.
[16] J. Chen, X. Wang, H. Han, *J. Nanopart. Res.* **2013**, *15*, 1–14.
[17] S. Gurunathan, J. W. Han, A. A. Dayem, V. Eppakayala, J.-H. Kim, *Inter. J. nanomed.* **2012**, *7*, 5901–5914.
[18] S. Sheshmani, M. Nayebi, *Polym. Compos.* **2019**, *40*, 210–216.
[19] J. Prakash, K. S. K. Venkataprasanna, D. Prema, S. M. Sahabudeen, S. Debashree Banita, G. D. Venkatasubbu, *Toxicol. Mech. Methods* **2020**, *30*, 508–525.
[20] S. Silver, L. T. Phung, *Annu. Rev. Microbiol.* **1996**, *50*, 753–789.
[21] Z. Wu, J. Luo, J. Zhang, H. Huang, Z. Xie, X. Xie, *Coating* **2021**, *11*, 716.
[22] Z. Xu, C. Zhang, X. Wang, D. Liu, *ACS Appl. Bio. Mater.* **2021**, *4*, 3985–3999.
[23] M. Catauro, M. Raucci, F. De Gaetano, A. Marotta, *J. Mater. Sci.* **2004**, *15*, 831–837.
[24] J. H. Crabtree, R. J. Burchette, R. A. Siddiqi, I. T. Huen, L. L. Hadnott, A. Fishman, *Peritoneal Dial. Int.* **2003**, *23*, 368–374.
[25] X. Meng, S. Tang, S. Vongehr, *J. Mater. Sci. Technol.* **2010**, *26*, 487–522.
[26] Y.-H. Chan, C.-F. Huang, K.-L. Ou, P.-W. Peng, *Surf. Coat. Technol.* **2011**, *206*, 1037–1040.
[27] Y. Yan, W. Kuang, L. Shi, X. Ye, Y. Yang, X. Xie, Q. Shi, S. Tan, *J. Alloys Compd.* **2019**, *777*, 234–243.
[28] H.-Y. Yang, Y.-W. Zhao, Z.-Y. Zhang, H.-M. Xiong, S.-N. Yu, *Nanotechnology* **2013**, *24*, 055706.
[29] J. Xiang, H. Cao, Q. Wu, S. Zhang, X. Zhang, A. A. Watt, *The J. Phy. Chem. C* **2008**, *112*, 3580–3584.
[30] X. Lu, X. Feng, J. R. Werber, C. Chu, I. Zucker, J.-H. Kim, C. O. Osuji, M. Elimelech, *Proc. Nat. Acad. Sci.* **2017**, *114*, E9793-E9801.
[31] C. Levard, E. M. Hotze, B. P. Colman, A. L. Dale, L. Truong, X. Yang, A. J. Bone, G. E. Brown Jr, R. L. Tanguay, R. T. Di Giulio, *Env. Sci. & technol.* **2013**, *47*, 13440–13448.
[32] M. Moritz, M. Geszke-Moritz, *Chem. Eng. J.* **2013**, *228*, 596–613

Submitted: April 27, 2021
Accepted: August 3, 2021